LIMNOLOGY and OCEANOGRAPHY

ASLO

Limnol. Oceanogr. 71, 2026, e70381

doi: 10.1002/lno.70381

RESEARCH ARTICLE

Molecular and optical signatures of labile dissolved organic matter during bloom senescence in the Amundsen Sea Polynya

Hui Lin [1*], **Qiang Hao** [2], **Wei Zhang** [2], **Zhenwei Yan** [3], **Hao Zhang** [1], **Ziming Fang** [4], **Yuan Gao** [1], **Yong Yu** [1], **Ding He** [3,5]

[1]Polar Research Institute of China, Shanghai, China; [2]Second Institute of Oceanography, Ministry of Natural Resources, Hangzhou, China; [3]Department of Ocean Science and Center for Ocean Research in Hong Kong and Macau, The Hong Kong University of Science and Technology, Hong Kong SAR, China; [4]State Key Laboratory of Marine Environmental Science, College of Ocean and Earth Sciences, Xiamen University, Xiamen, China; [5]Sanya Joint Laboratory of Marine Science Research, The Hong Kong University of Science and Technology, Hong Kong SAR, China

Abstract

The Amundsen Sea Polynya (ASP) in the Southern Ocean serves as a potentially significant carbon sink, where phytoplankton blooms drive intense primary production and dissolved organic matter (DOM) cycling. This study focuses on DOM dynamics during the late-summer bloom phase dominated by *Phaeocystis antarctica*. Despite the ASP's high productivity, DOM characteristics and their response to bloom senescence remain poorly resolved, limiting insights into carbon sequestration efficiency. We integrated absorbance and fluorescence spectroscopy with Fourier transform ion cyclotron resonance mass spectrometry to analyze seawater samples collected along transects in the ASP during austral summer 2022. Key findings include non-exponential chromophoric DOM spectra with distinct shoulders at 270–290 nm (aromatic amino acids) and 300–350 nm (mycosporine-like amino acids), elevated protein-like fluorescent DOM components linked to *P. antarctica* degradation, and enrichment of labile, low-molecular-weight compounds (< 350 Da) with increased sulfur-containing molecules from dimethylsulfoniopropionate oxidation. Bloom decline featured high dissolved organic carbon (0.85 ± 0.14 mg·L^{-1}) amid reduced chlorophyll a (3.81 ± 0.77 mg·m^{-3}), indicating DOM release under iron-replete, nitrate-limited conditions. This work advances knowledge by identifying unique phytoplankton-derived DOM signatures that challenge conventional optical metrics like spectral slopes in polar systems, highlighting autochthonous production over terrestrial inputs. Broader implications include improved predictions of carbon cycling in expanding polynyas under climate change, emphasizing reduced sequestration due to labile DOM remineralization and its vulnerability to warming-induced shifts in Antarctic ecosystems.

Antarctic coastal polynyas, dynamic regions of open water surrounded by sea ice, are critical yet understudied components of the Southern Ocean's role in the global carbon cycle (Williams et al. 2007; Mohrmann et al. 2021). These ecosystems act as hotspots for primary production, driving both biological activity and carbon dioxide sequestration, thereby contributing disproportionately to the Southern Ocean's carbon sink (Arrigo et al. 2008). Among these polynyas, the Amundsen Sea Polynya (ASP) stands out as the fourth largest polynya in Antarctica (Macdonald et al. 2023) and the most productive, with net primary production rates reaching 2.5 g C m^{-2} d^{-1} (Arrigo and van Dijken 2003; Arrigo et al. 2012). Climate models predict the ASP will expand as atmospheric and oceanic warming accelerates, potentially amplifying its carbon sequestration capacity (Arrigo and van Dijken 2003). However, the efficiency of this process is modulated by complex biogeochemical interactions, particularly the response of dissolved organic matter (DOM) to seasonal phytoplankton blooms—a critical yet poorly constrained aspect of carbon cycling in the region. Despite its high productivity, the ASP sequesters only a small fraction of its sinking carbon. More than 95% of photosynthetic particulate organic matter was converted to suspended POM and DOM in the upper 400 m layer (Lee et al. 2017).

*Correspondence: linhui@pric.org.cn

Associate editor: Florence Schubotz

This limited sequestration rate arises from the intrusion of Circumpolar Deep Water (CDW), which flows onto the Amundsen Shelf, mixes with overlying waters to form modified CDW (mCDW), and flushes out back to the Southern Ocean. While CDW intrusion supplies large amounts of nutrients, including iron, to sustain phytoplankton growth, light availability ultimately constrains the massive austral summer blooms dominated by *Phaeocystis antarctica* (Park et al. 2017). Unlike the Ross Sea's dual blooms, the ASP sustains a single, intense bloom annually between December and February, creating a unique biogeochemical regime with distinct DOM production and transformation pathways (Macdonald et al. 2023; Smith and Trimborn 2024).

Fluorescence spectroscopy has revealed that autochthonous DOM dominates surface waters in the ASP, yet humic-like components, the tracers of CDW, persist throughout the water column (Chen et al. 2019; Jeon et al. 2021; Hu et al. 2023). Intriguingly, deep-water DOM in the ASP exhibits unexpected bioreactivity, with dissolved organic carbon (DOC) serving as a substrate for microbial activity (Fang et al. 2020). However, molecular-level insights remain sparse. While Fourier transform ion cyclotron resonance mass spectrometry (FT-ICR-MS) studies in Prydz Bay (Jiang et al. 2024) and a bulk mixed sample from the ASP (Chen et al. 2019) have identified labile DOM components, the spatial and temporal heterogeneity of DOM composition remains unresolved. These gaps hinder efforts to link DOM dynamics to carbon export efficiency in a warming climate.

This study investigates the quantity, optical properties, molecular composition, sources, and fate of DOM in the ASP during the austral summer phytoplankton bloom. We combine chromophoric DOM (CDOM) absorption and fluorescence spectroscopy with FT-ICR-MS to (1) quantify the relative contributions of autochthonous (e.g., phytoplankton exudates) and allochthonous (e.g., CDW-derived) DOM, (2) assess the bioreactivity of DOM pools, and (3) evaluate how climate-driven changes, including CDW intrusion, sea ice melt, and polynya expansion, modulate DOM cycling. By resolving these processes, our work advances understanding of the ASP's role in the global carbon cycle and provides a framework for predicting carbon sequestration responses to Antarctic ecosystem shifts under climate change.

Method

Study areas and water masses

The Amundsen Sea was surveyed on board R/V icebreaker *Xuelong* during the austral summer from January 24th to February 18th, 2022 (Fig. 1a). The hydrology in the Amundsen Sea has been extensively described (Jacobs et al. 2012; Turner et al. 2017; Golledge et al. 2025). Briefly, Circumpolar Deep Water (CDW), a warm and saline water mass circulating around the Southern Ocean with poor dissolved oxygen, intrudes onto the bottom of the ASP via the Dotson-Getz Trough, supplying heat and nutrients (Fig. 1a). It mixes with the ASP shelf water, forming the modified CDW (mCDW). Sea-ice melting desalted the surface water, leaving colder, saltier Winter Water in the mid-layer of the ASP water column (Fig. 1b). Sampling stations were categorized based on the sea ice concentration and geographic location (Fig. 2a): the Amundsen Sea Open Water (OW, sea ice concentration < 10% and west of 120°W), the sea ice-covered areas (SIC, sea ice concentration > 10% and west of 120°W), and the polynya (ASP, east of 120°W).

Sample collection

Seawater samples (~ 6 L) were collected using Niskin bottles mounted on a SBE 911 plus CTD rosette. Sampling locations for Chl *a*, CDOM, and FDOM are shown in Fig. 1a. For FT-ICR MS analysis and incubation experiments (phytoplankton growth rate and photosynthetic efficiency), samples were collected along an east-to-west transect spanning from the Amundsen Sea open water to the ASP (Fig. 2a). Hydrographic conditions, including temperature and salinity for this transect, are provided in Supporting Information Fig. S1. Immediately after collection, 2 L of seawater were allocated for incubation experiments. The remaining 4 L were filtered onboard through pre-combusted (450°C, 4 h) GF/F filters (Whatman, 0.7 μm pore size) for particulate organic carbon (POC) analysis. The filtrate was stored in pre-combusted (450°C, 4 h) amber borosilicate glass vials (60 mL for CDOM and FDOM, 40 mL for DOC) and preserved at −20°C in the dark until laboratory analysis. Although freezing can potentially alter DOM optical properties through aggregation or conformational changes (Spencer et al. 2007), all samples were subjected to identical storage conditions, and only a single thaw was performed prior to analysis to minimize freeze–thaw artifacts. Thus, observed spatial patterns are considered robust for comparative purposes.

Particulate and dissolved organic carbon concentration

Particulate organic carbon concentrations were measured post-cruise. GF/F filters were exposed to HCl fume for 12 h to remove the inorganic carbon, dried in 50°C condition, and analyzed using a Vario Micro Cube element analyzer (Elementar, German). Dissolved organic carbon concentrations were determined using a Shimadzu TOC-L analyzer based on high temperature combustion method. Instrument accuracy was verified every six samples using Milli-Q water (blank) and a deep-water reference from the Florida Strait (42–45 μM-C, University of Miami).

Chromophoric dissolved organic matter and fluorescent dissolved organic matter

Filtrate samples were thawed to room temperature, and FDOM was measured using an Aqualog spectrofluorometer (Horiba, Japan). Excitation-emission matrices (EEMs) were generated over excitation wavelengths of 250–450 nm (5 nm intervals) and emission wavelengths of 300–600 nm (2 nm

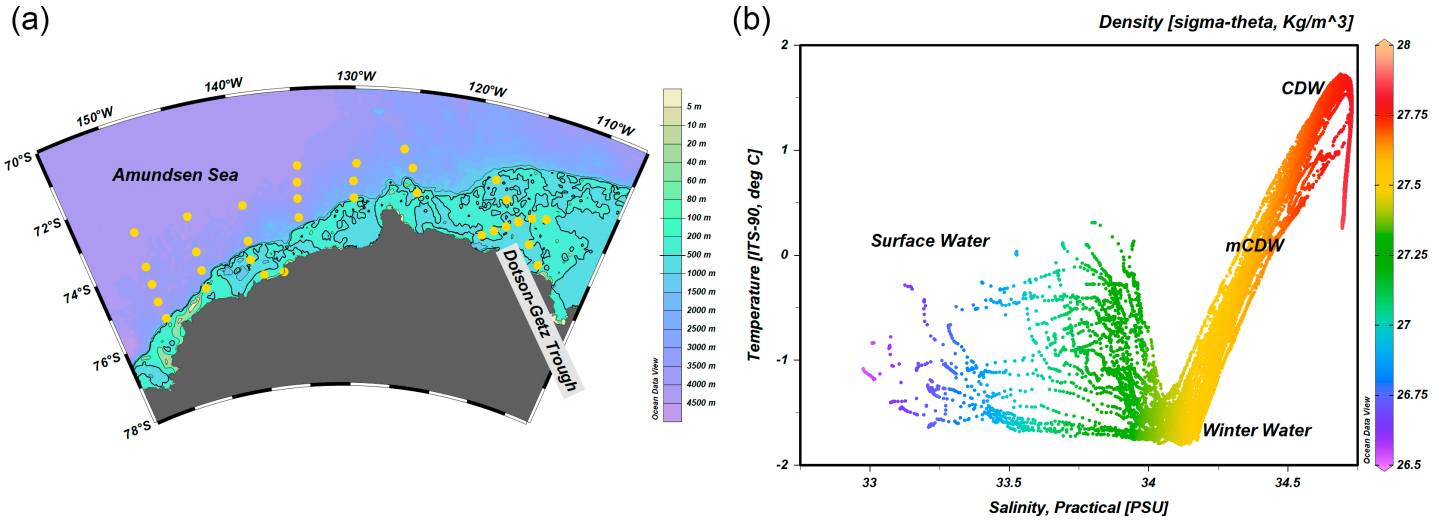

Fig. 1. (**a**) Map of the Amundsen Sea showing topography with sampling stations (yellow dots). (**b**) Temperature-salinity diagram for the Amundsen Sea, color-coded by density ($\sigma\theta$, kg/m^3), highlighting Surface Water, Winter Water, modified Circumpolar Deep Water (mCDW), and Circumpolar Deep Water (CDW) water masses.

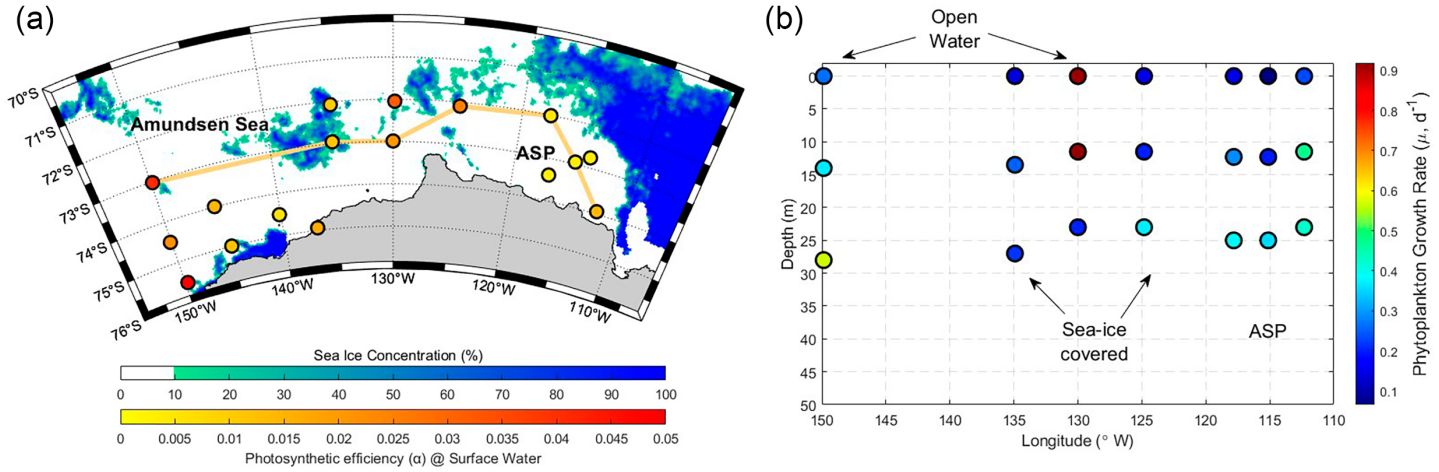

Fig. 2. (**a**) Map of the Amundsen Sea Polynya (ASP) region showing sea ice concentration (%) and photosynthetic efficiency (α) at surface water, with sampling stations of SPE-DOM along a transect (yellow line). The sea ice concentration data is downloaded from research group "remote sensing of polar regions" at the University of Bremen (Ludwig et al. 2020). (**b**) Section distribution of phytoplankton growth rate (μ, d^{-1}) across the transect shown in (a) panel.

intervals). Parallel factor analysis (PARAFAC) was performed to resolve the EEM spectra using the "drEEM" toolbox (v.0.5) on Matlab (R2022a, Murphy et al. 2013). Split-half validation and random initialization validation were carried out to validate a model. Both the four-component model and the five-component model passed the split-half validation and the random initialization validation. However, the sum of errors calculated from the five-component model was significantly lower than that from the four-component model (Supporting Information Fig. S6). Therefore, the five-component model was selected as the final model. Components were labeled using the notation $C_{X/Y}$, where X and Y denote the peak excitation and emission wavelengths (in nm), respectively. Chromophoric dissolved organic matter absorbance spectra were measured simultaneously using the AquaLog spectrofluorometer (240–900 nm, 0.2 nm intervals), with Milli-Q water as the blank. The absorption coefficient (a_λ) was calculated as: $a_\lambda = 2.303^* A_\lambda / l$, where A_λ is the absorbance at wavelength λ, and l is the cuvette length in meters.

Solid phase extraction and Fourier transform ion cyclotron resonance mass spectrometry analysis

A total of 35 solid-phase extraction of dissolved organic matter (SPE-DOM) samples were collected from 7 stations

across the Amundsen Sea and the ASP, including OW, SIC, and ASP from west to east (Fig. 2). At each station, seawater was collected from five depths corresponding to distinct photochemical and biological zones: the 100%, 10%, and 1% light-saturated surface layers, as well as at 100 m, 200 m. Complementary measurements of photosynthetic efficiency and phytoplankton growth rates were also obtained from the same water columns, which are described in the following section.

Dissolved organic matter (DOM) was extracted from 4 L of 0.2-μm filtered seawater using PPL cartridges (Agilent Bond Elut, 500 mg), which were pre-conditioned with one cartridge volume of HPLC-grade methanol (Sigma-Aldrich), followed by acidification of the seawater sample to pH 2 with 6 M HCl. The acidified sample was then loaded onto the cartridge at a flow rate of < 6 mL min^{-1}. After loading, cartridges were rinsed with two volumes of acidified (pH 2) Milli-Q water to remove residual salts and subsequently eluted with one cartridge volume of HPLC-grade methanol. The methanol eluates (SPE-DOM) were stored at -20°C in the dark until analysis. Solid phase extraction recovery efficiency, determined from pre- and post-extraction DOC measurements ($n = 35$), averaged 35.7% ± 6.1% (25.3%–48.0%), consistent with PPL-based DOM extractions in marine systems (Dittmar et al. 2008).

All SPE-DOM samples were analyzed using a Bruker 15 T solariX FT-ICR MS equipped with an electrospray ionization (ESI) source, operated in negative ionization mode. Each sample was infused at a flow rate of 120 μL h^{-1} via syringe pump, and 128 scans were accumulated per analysis to enhance signal-to-noise ratio. Mass calibration was performed externally using a series of well-established DOM-relevant standard compounds within the Bruker Compass DataAnalysis 5.0 software suite. Molecular formulas were assigned (mass error < 1 ppm) with elemental compositions of $^{12}C_{1–100}{}^{1}H_{1–200}{}^{16}O_{1–50}{}^{14}N_{0–3}{}^{31}P_{0–1}{}^{32}S_{0–2}$ (Yi et al. 2023) and a signal-to-noise thresholds > 6. Molecular characteristics were visualized via van Krevelen diagrams (H/C vs. O/C) and classified by:

1. Modified aromaticity index (AI_{mod}) (Koch and Dittmar 2006, 2016).
2. Double bond equivalents ($DBE = 1 + 0.5[2C - H + N + P]$).
3. Nominal Oxidation State of Carbon ($NOSC = -[(4C + H - 3N - 2O + 5P - 2S)/C] + 4$) (LaRowe and Philippe 2011).

Biogeochemical indices included:

1. Degradation index (I_{DEG}; higher value = higher degradation state) (Flerus et al. 2012).
2. Molecular labile boundary (MLB_L; higher values = greater biodegradability) (D'Andrilli et al. 2015).

Compounds are classified as polycyclic condensed aromatics ($AI_{mod} \geq 0.67$), highly aromatic compounds with aliphatic side chains ($0.5 \leq AI_{mod} \leq 0.66$), highly unsaturated compounds with soil derived products ($AI_{mod} < 0.5$ and $H/C < 1.5$), unsaturated aliphatic compounds ($1.5 < H/C \leq 2$ and $N = 0$), saturated compounds with lipids ($H/C > 2$ and $O/C < 0.9$), saturated compounds with carbohydrate ($H/C > 2$ and $O/C > 0.9$), and unsaturated aliphatic compounds with N include peptide ($1.5 \leq H/C < 2$ and $N > 0$) (Seidel et al. 2015) as well as carboxyl-rich alicyclic molecules (CRAM, $DBE/C = 0.3–0.68$, $DBE/H = 0.2–0.95$ and $DBE/O = 0.77–1.75$, Hertkorn et al. 2006). Although FT-ICR-MS offers high molecular resolution, the SPE-based approach captures only a subset of DOM. PPL resin retains hydrophobic and medium-polarity compounds but excludes highly polar, ionic, and low–molecular-weight metabolites (e.g., free amino acids, organic acids, sugars), many of which are the most labile and bioavailable. Thus, our "labile" signatures (e.g., protein-like compounds, lipids, < 350 Da molecules) represent the most reactive fraction within the extractable DOM pool, not the full spectrum of bioavailable DOM in seawater.

Chl *a* concentration, photosynthetic efficiency, and phytoplankton growth rate

Water samples were filtered through 0.7 μm GF/F filters. Chl *a* was extracted using 90% acetone in dark conditions for 12 h. Then it was measured on a Turner 10-AU fluorometer, which is calibrated against Chl *a* standard (Sigma-Aldrich) prior to the cruise.

The photosynthesis efficiency (α) and the phytoplankton daily growth rate (μ) are calculated based on photosynthesis-irradiance (*P–E*) experiments. *P–E* experiments were conducted onboard in incubators housing eight 75 mL glass culture flasks illuminated by LED lamps. Water samples were inoculated with 5 μCi of ^{14}C labeled bicarbonate and maintained at in situ sea temperature (~ -2°C) using a cooling pump machine. After 1–2 h of incubation, the particulate material was filtered through 25 mm Whatman GF/F filters. The filters were folded, stored in custom plates, evacuated, and frozen. After the cruise, filters were fumed with HCl fume for 12 h, and radiocarbon activities were measured using a liquid scintillation analyzer. The light-saturated Chl *a* and the light limited slope α and β were estimated by fitting the data to the following model using a nonlinear least-squares regression (Lewis et al. 2019):

$$P_z = P_s\left(1 - e^{\frac{-\alpha E_{PAR}}{P_s}}\right)e^{\frac{-\beta E_{PAR}}{P_s}}$$

where P_z is the Chl *a*-specific rate of photosynthesis (mgC mg^{-1} Chl *a* h^{-1}), the P_s is the light-saturated rate of photosynthesis (mgC mg^{-1} Chl *a* h^{-1}), E_{PAR} is the photosynthetically active irradiance (μEin m^{-2} s^{-1}). α is the initial slope of the *P–E* curve, which can indicate the photosynthesis efficiency (mgC mg^{-1} Chl *a* h^{-1} [μEin m^{-2} s^{-1}]$^{-1}$), and β is the coefficient of photoinhibition (mgC mg^{-1} Chl *a* h^{-1} [μEin m^{-2} s^{-1}]$^{-1}$). The phytoplankton daily growth rate (μ; d^{-1}) can be calculated using the *P–E* parameters

$$\mu = \frac{\alpha \cdot E_{PAR}}{\mathrm{POC} : \mathrm{Chl}\,a} \times 24$$

Statistical analysis

Mann–Whitney *U* tests were performed to assess differences in parameter distributions between regional categories (OW, SIC, ASP) for both environmental parameters and molecular characteristics (Supporting Information Table S2). To address the multiple comparisons across multiple region pairs, the Benjamini–Hochberg procedure was implemented to control the false discovery rate (FDR) at $\alpha = 0.05$. This approach provides a less conservative correction compared to family-wise error rate methods (e.g., Bonferroni correction), optimizing the balance between Type I and Type II error rates in multiple hypothesis testing scenarios. Effect sizes were quantified using the rank-biserial correlation to assess the magnitude of observed differences between regional groups. All statistical analyses were conducted using Python with SciPy and statsmodels packages. Statistical significance was defined as FDR-adjusted *p*-values < 0.05.

Results

Chl *a* concentration spatial distribution

During the study period (late January to mid-February), Chl *a* concentration ranged from 0.46 to 5.45 mg·m^{-3}, with the highest values (2.58–5.45 mg·m^{-3}) observed in the ASP. Mean Chl *a* level in the ASP (3.81 ± 0.77 mg·m^{-3}) was significantly higher than those in the OW area (1.29 ± 0.68 mg·m^{-3}) and IC regions (1.21 ± 0.33 mg·m^{-3}) ($p < 0.05$). Coastal onshore areas also showed elevated Chl *a* concentration (3.7 ± 0.93 mg·m^{-3}), with vertical profiles indicating maxima within the 0–50 m mixed layer due to strong stratification. In contrast, the well-mixed ASP exhibited a deeper chlorophyll-cline at 75–100 m depth.

Field observations indicated a greenish discoloration of the water column and dense phytoplankton aggregations (Supporting Information Fig. S2). Vertical net tows collected high biomass accumulations of *P. antarctica*, sufficient to clog net meshes. These Chl *a* levels suggest that the sampling period captured the late stage of an algal bloom, with concentrations lower than historical bloom peaks (~ 20 mg·m^{-3}) reported in the ASP from mid-December 2010 to early January 2011 (Arrigo et al. 2012) and an order of magnitude below peak levels observed from mid-January to early February 2016 (Chen et al. 2019).

Photosynthetic efficiency (α) and phytoplankton growth rate (μ)

Surface photosynthetic efficiency (α) varied significantly across regions, with the highest values in open water and the lowest in the polynya ($p < 0.05$; Fig. 2a). Similarly, phytoplankton growth rates (μ) peaked in open water (e.g., 0.91 d^{-1} at the surface of Station A1), exceeding averages in ice-covered areas (0.30 ± 0.12 d^{-1}) and the ASP (0.27 ± 0.09 d^{-1}). Notably, μ values at 10% and 1% light depths in the polynya and open water exceeded those in surface layers, indicating that light availability alone does not constrain the phytoplankton growth in these regions (Fig. 2b). The parallel low α and μ values within the polynya suggests that the reducing of light exposure caused by the *P. antarctica* bloom may limit photosynthetic efficiency and growth rate.

Particulate organic carbon and dissolved organic carbon

Particulate organic carbon concentrations spanned 12.32–221.58 μg·L^{-1}, peaking in surface waters (< 200 m) across the transect (Fig. 3). While polynya POC (e.g., 1.29 ± 0.68 μg·L^{-1}) did not differ significantly from other regions, DOC was elevated in the ASP (0.848 ± 0.135 mg·L^{-1} vs. 0.659 ± 0.084 mg·L^{-1} in non-polynya waters; $p < 0.05$). This disparity suggests *P. antarctica*-derived DOM release during bloom senescence, consistent with post-bloom shifts from particulate to DOC pools.

Chromophoric dissolved organic matter

Absorbance spectra revealed atypical features for marine DOM: a prominent shoulder peak at 250–290 nm, maxima at 260 nm (red spectrum in Fig. 4), and a secondary peak at 300–350 nm, maximum at 340 nm (yellow spectrum in Fig. 4), and a third small peak at maximum 450 nm (green spectrum in Fig. 4). Thus, we choose a_{260}, a_{340}, and a_{450} as example for the surface distribution (Supporting Information Fig. S3). In the surface water, CDOM a_{320} and a_{450} in the ASP is significantly higher than those in Amundsen Sea open water and ice-covered area ($p < 0.05$), and coastal area is significantly higher than offshore area ($p < 0.05$). This is basically

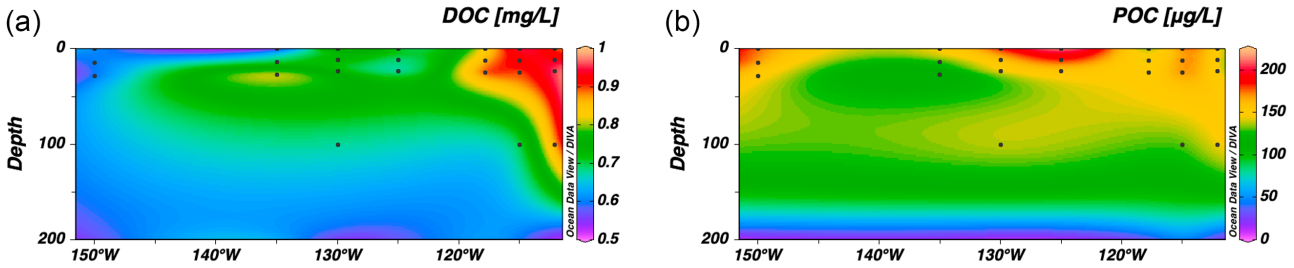

Fig. 3. Section distribution of (**a**) dissolved organic carbon concentration and (**b**) particulate organic carbon concentration.

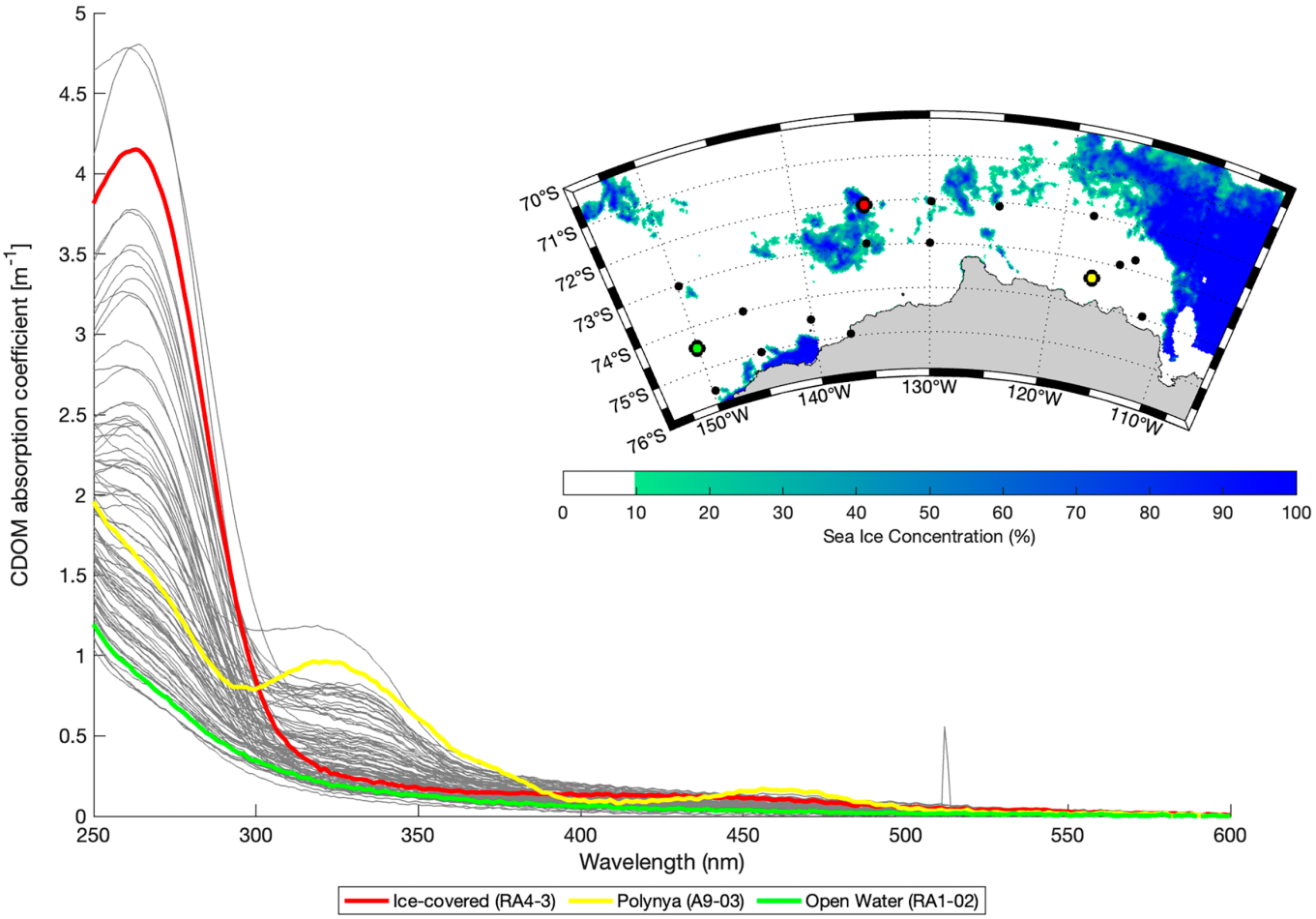

Fig. 4. Absorption spectra of chromophoric dissolved organic matter (CDOM). The red, yellow, and green lines denote representative spectra for ice-covered area, polynya area, and open water area, respectively.

consistent with previous observations (Chen et al. 2019; Hu et al. 2023).

Absorbance spectra of ASP DOM exhibited distinct spectral features, including a prominent shoulder between 250 and 290 nm (maximum ~ 260 nm; red spectrum in Fig. 4), a secondary peak between 300 and 350 nm (maximum ~ 320 nm; yellow spectrum), and a minor feature near 450 nm (green spectrum). While such spectral shoulders and peaks are sometimes interpreted as indicators of mycosporine-like amino acids (MAAs) or other photoprotective compounds in marine systems, UV–Vis absorbance alone cannot definitively identify specific molecular classes (e.g., MAAs vs. aromatic amino acid derivatives, polyphenols, or photochemical degradation products, Chen and Jaffé 2016). These features are also commonly observed in DOM derived from biomass and soil leachates, reflecting the complex and heterogeneous nature of CDOM in aquatic environments.

For comparative purposes, we selected a_{260}, a_{320}, and a_{450} as representative wavelengths to illustrate spatial trends (Supporting Information Fig. S3). In surface waters, CDOM absorbance at a_{320} and a_{450} was significantly higher in the ASP compared to open Amundsen Sea waters and ice-covered regions ($p < 0.05$), and coastal areas showed significantly higher values than offshore zones ($p < 0.05$). These patterns align with prior observations in the region (Chen et al. 2019; Hu et al. 2023), likely reflecting elevated DOM loading and altered composition associated with intense phytoplankton blooms and lateral transport from productive polynya interiors.

Fluorescent dissolved organic matter

Parallel factor analysis resolved five fluorescence components ($C_{260/288}$, $C_{270/324}$, $C_{265/436}$, $C_{250/368}$, $C_{275/340}$) in the ASP (Supporting Information Fig. S4). The protein-like components $C_{260/288}$, $C_{270/324}$, and $C_{275/340}$ exhibited weak pairwise correlations ($r < 0.3$; Supporting Information Fig. S5) and limited matches in the OpenFluor database (Supporting Information Table S1). $C_{270/324}$ and $C_{275/340}$, with similar excitation (270 and 275 nm) and emission wavelengths (324 and 340 nm), likely correspond to tryptophan or tryptophan-like

amino acids, such as glycoproteins (Wormald and Dwek 1999), which are strongly associated with the degradation of the *P. antarctica*-dominated bloom. $C_{260/288}$ is potentially associated with tyrosine or tyrosine-like amino acids. Aggregated due to their shared protein-like nature, these components showed elevated concentrations in ASP surface waters (Fig. 5), reflecting labile DOM production during bloom senescence. In contrast, the humic-like component $C_{265/436}$, consistent with prior ASP studies (Chen et al. 2019; Hu et al. 2023), was enriched in Circumpolar Deep Water (CDW)-influenced layers and diminished in polynya surface waters. The novel $C_{250/368}$ component, characterized by an M-peak and lacking literature precedents, displayed higher intensities in open-ocean surface waters, suggesting links to pelagic processes or photodegradation products (Fig. 5). While $C_{275/340}$ resembles glacial-derived fluorophores reported by (Chen et al. 2019), its prevalence in the ASP correlated with iron-mediated *P. antarctica* blooms, though distinguishing between glacial meltwater and phytoplankton sources requires targeted biomarker validation. This spatial partitioning highlights the ASP's dominance in labile DOM production during bloom senescence, contrasting with refractory humic-like signals in deeper, CDW-affected layers.

Fourier transform ion cyclotron resonance mass spectrometry molecular signatures

Solid-phase extraction of dissolved organic matter was analyzed using FT-ICR MS, which identified 10,980 unique molecular formulas totally (4972–7089 per sample, averagely 6070 ± 516). It is important to note that this analysis reflects only the hydrophobic to medium-polarity fraction of DOM, as SPE excludes highly polar and ionic compounds (e.g., free amino acids, organic acids), and electrospray ionization in negative mode favors acidic, carboxyl-rich, and aromatic molecules. Consequently, the observed molecular patterns represent relative trends within the extractable DOM pool rather than absolute descriptors of bulk seawater DOM.

Given the impracticality of displaying all VK diagrams, we selected two representative samples to illustrate DOM molecular characteristics in the Amundsen Sea and ASP: (1) surface water from ASP (Station A11-00, Supporting Information Fig. S1), close to the Thwaites Glacier, a major source of glacial meltwater input to the polynya, (2) open water from the Amundsen Sea influenced by CDW intrusion at the 200 m depth, which exhibits high-temperature, high-salinity features (Supporting Information Fig. S1). Comparative analysis revealed distinct DOM molecular composition differences between these two samples. Surface ASP DOM (Fig. 6 left panel) displays higher aliphatic content (H/C > 1.5), dominated by lipid-like (O/C < 0.3), protein-like (O/C 0.3–0.6), and carbohydrate-like (O/C 0.6–1.2) compounds, while CDW-influenced deep water (Fig. 6, right panel) exhibits a more refractory molecular signature, consistent with its older, more processed DOM pool.

Aromaticity indices revealed distinct spatial patterns: ASP water columns showed lower DBE_{wa}, AI_{mod}, $NOSC_{wa}$, and m/z_{wa} ratios compared to open-water and ice-covered regions, where aromaticity was elevated (Fig. 7a–e). Molecular lability indices further differentiated ASP DOM: elevated MLB_L(20.2% ± 2.3% in ASP vs. 17.0% ± 2.1%in ice-covered areas and 17.8 ± 2.4 in the open water), lower CRAM percentage and lower I_{DEG} confirmed fresher, more labile DOM (e.g., lipid exudates) in the ASP (Fig. 7g–h). These patterns

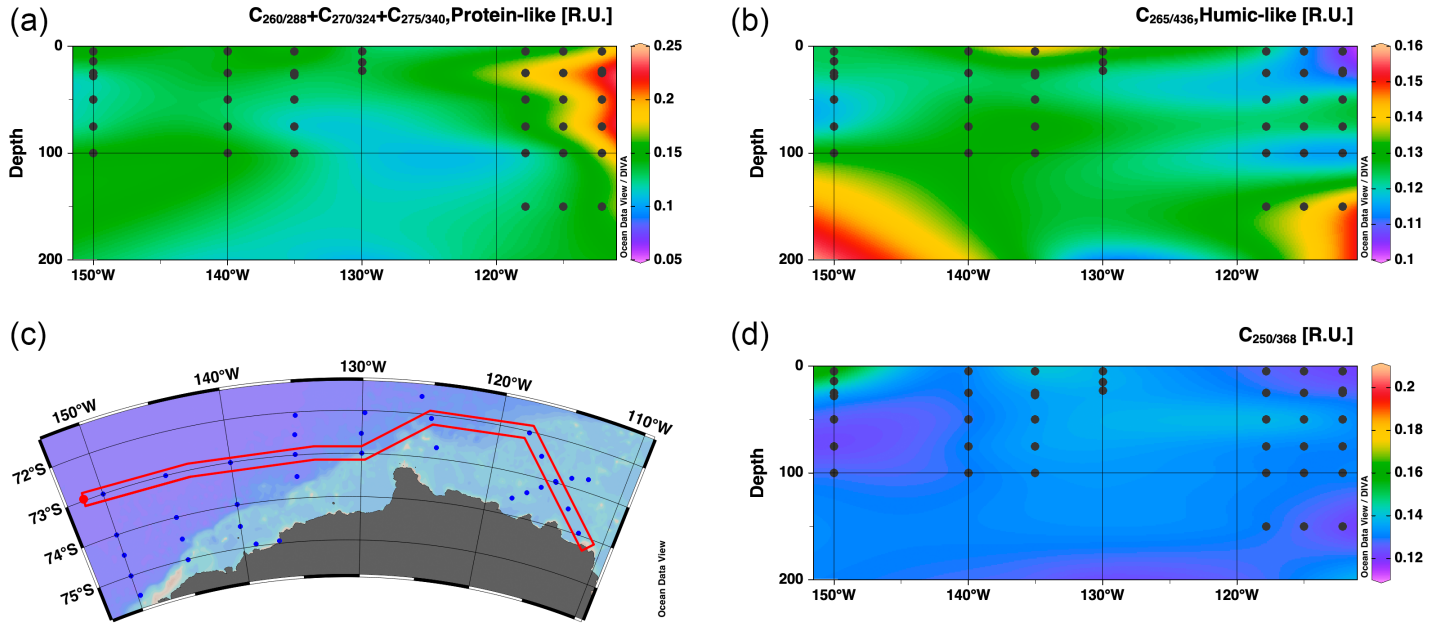

Fig. 5. Section distribution of five fluorescence DOM components along the section. (**a**) All protein-like $C_{260/288}$, $C_{270/324}$ and $C_{275/340}$ are aggregated together. (**b**) The humic-like component $C_{265/436}$. (**c**) The map and the section. (**d**) The component $C_{250/368}$.

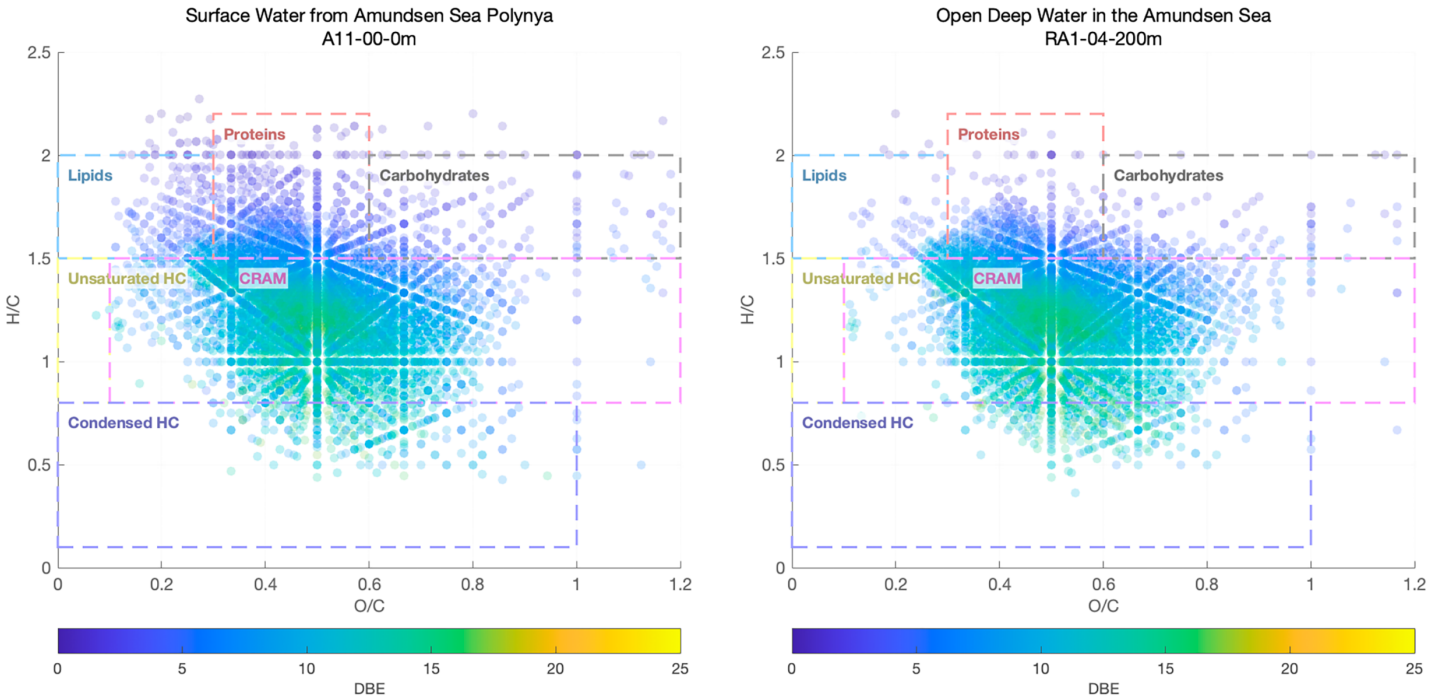

Fig. 6. Van Krevelen (VK) diagram for dissolved organic matter (DOM) samples collected from surface water of the Amundsen Sea Polynya (left panel) and open water in the Amundsen Sea (right panel). Characteristic molecular groups are outlined by colored rectangles: cyan (lipids), red (proteins), black (carbohydrates), yellow (unsaturated hydrocarbons), pink (Carboxyl-Rich Alicyclic Molecules, CRAM), and blue (condensed hydrocarbons).

contrast sharply with refractory DOM in open waters (D'Andrilli et al. 2015), underscoring the ASP's role as a hotspot for rapid organic matter cycling during bloom senescence.

Discussion

Environmental controls on phytoplankton dynamics in the last-stage bloom

Late summer sampling (3–7 February) captured the terminal phase of the ASP monocultural bloom, dominated by *P. antarctica*, distinct from the Ross Sea's dual bloom regime (Smith and Trimborn 2024). Chl *a* in the ASP (3.81 ± 0.77 mg·m^{-3}) exceeded those in non-polynya regions but was an order of magnitude lower than historical peak values (~ 20 mg·m^{-3}; Arrigo et al. 2012), confirming bloom senescence. The Chl *a* levels are consistent with prior 16 yr observations (Park et al. 2017). Low photosynthetic efficiency ($\alpha = 0.27 \pm 0.09$ d^{-1}) and phytoplankton growth rates ($\mu \approx 0.31$ d^{-1}; Lee et al. 2022) further indicate declining physiological activity, typical of late-stage *P. antarctica* bloom. Notably, higher growth rates at 10% and 1% light levels compared to 100% surface irradiance suggest that light availability is not the primary limiting factor during this period.

While Park et al. (2017) highlight light as a key limiter over iron during bloom peak, and Lee et al. (2022) emphasize solar radiation's role, these studies focus on the bloom's flourishing phase. In contrast, our late-season observations suggest that nitrate availability, in conjunction with light attenuation due to self-shading, likely constrained phytoplankton growth during bloom decline. As nutrient concentrations were not directly measured in this study, our inferences regarding nutrient limitation are based on physiological parameters and supported by previous literature. Specifically, multiple studies report near-complete nitrate (or dissolved inorganic nitrogen, DIN) drawdown by the end of the ASP bloom (Yager et al. 2012; Smith and Trimborn 2024). Given *P. antarctica*'s strong preference for nitrate over reduced nitrogen forms, the presence of ammonium, suggested by a sulfidic/ammoniacal odor during sampling, may not sustain growth. Moreover, elevated growth rates in deeper waters (Fig. 2b) likely reflect access to nitrate supplied by modified Circumpolar Deep Water (mCDW), whereas surface waters were isolated by strong stratification, limiting vertical nutrient replenishment. Together, these lines of indirect evidence point to nitrate and light as co-limiting factors during the late-stage ASP bloom, though future studies with concurrent nutrient profiling are needed to confirm this hypothesis.

Chromophoric dissolved organic matter absorbance characteristics

The absorbance spectra in the ASP exhibit distinct shoulder peaks at 270–290 nm and 300–350 nm, consistent with phytoplankton-derived DOM characteristics. While similar features have been attributed to both phytoplankton and krill

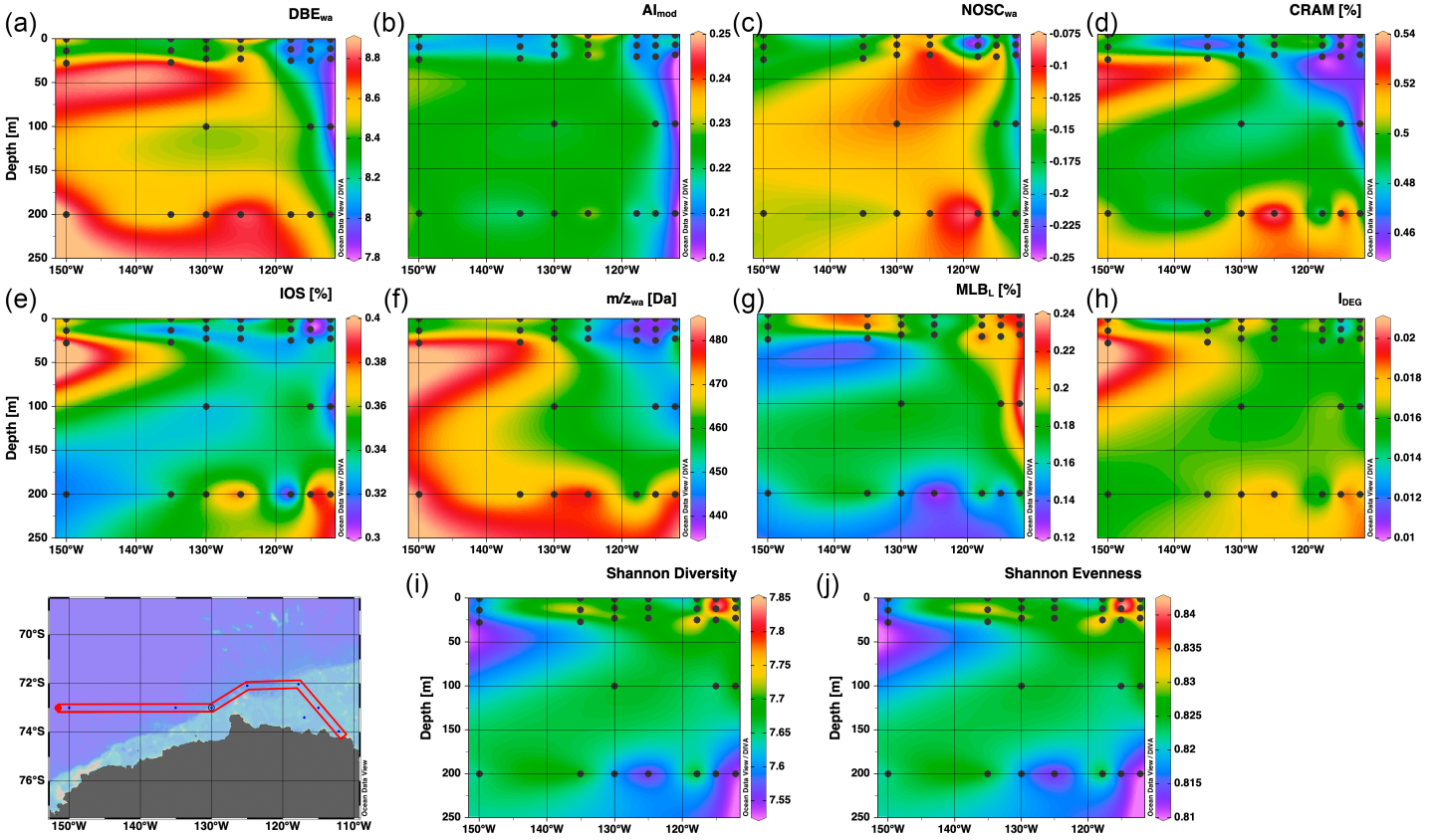

Fig. 7. Section distribution of (**a**) double bond equivalents (DBE_{wa}), (**b**) Aromaticity Index modified (AI_{mod}), (**c**) Nominal Oxidation State of Carbon ($NOSC_{wa}$), (**d**) Carboxyl-Rich Aliphatic Matter (CRAM[%]), (**e**) Island of Stability (IOS[%]), (**f**) mass to charge ratio (m/z_{wa}), (**g**) Molecular lability boundary (MLB_L[%]), (**h**) degradation index (I_{DEG}), (**i**) Shannon Diversity, and (**j**) Shannon Eveness.

(*Euphausia superba*) in the Southern Ocean (Steinberg et al. 2004; Ortega-Retuerta et al. 2009; D'Sa et al. 2021), we exclude krill-derived contributions in the ASP due to the absence of significant krill swarms (Ross et al. 2004; Li et al. 2025), though they may still remain relevant in the IC area and OW areas.

The 270–290 nm shoulder peak likely reflects proteins, such as lectins, fibrillins, glycoproteins, actin, and tubulin, released during the late-stage *P. antarctica* bloom (Bender et al. 2018; Smith and Trimborn 2024; Fig. 4, ice-covered). The 300–350 nm shoulder aligns with mycosporine-like amino acids (MAAs), photoprotective compounds with microbial residence times of less than 48 h (Riegger and Robinson 1997; Shen and Benner 2019), and is consistent with *P. antarctica* absorbance profiles, distinct from open-ocean and ice-covered regions. Notably, flavodoxin (oxidized state peak at 373 nm), a protein substituting for metallo-enzymes in iron-sparing strategies, may also contribute to this signal (Bender et al. 2018). The transient nature of these peaks, particularly MAAs, necessitates immediate sample preservation to capture these ephemeral CDOM signals and accurately resolve in situ phytoplankton contributions. Consequently, a_{260} and a_{320} may serve as more reliable indicators of *P. antarctica* blooms than the commonly used a_{254} (Fig. S2).

Although DOC, protein-like FDOM, and MLB_L are all elevated in the ASP, their pairwise correlations are moderate and not statistically significant ($p > 0.05$), but CDOM a_{320} shows strong and significant correlations with molecular lability indices, including MLB_L ($r = 0.39$, $p < 0.05$), AI_{mod} ($r = -0.45$, $p < 0.05$), and NOSC ($r = -0.44$, $p < 0.05$). This indicates that CDOM a_{320} in the ASP is chemically coupled to the labile, aliphatic DOM produced during *P. antarctica* bloom senescence, likely due to aromatic amino acids and photoprotective metabolites (e.g., MAAs).

Unlike terrestrial-influenced aquatic systems with exponentially decaying CDOM spectra, the ASP's phytoplankton-driven absorbance spectra resist conventional parameterization using spectral slope metrics (e.g., $S_{275-295}$). This divergence highlights the Antarctic's unique DOM cycling, driven by intense seasonal autochthonous production and minimal terrestrial inputs from ice-covered soils and sparse vegetation. While spectral slopes effectively characterize refractory terrestrial DOM in global oceans, their utility

is limited in Antarctic polynya systems dominated by labile DOM.

Dissolved organic matter response to the bloom senescence and the dissolved organic matter-sulfur dynamics in the Amundsen Sea Polynya

The response of DOM to bloom senescence in the ASP reveals three characteristic patterns. First, we observe elevated DOC concentrations (0.848 ± 0.135 mg/L) in the polynya's mixed layer (< 200 m, $p < 0.05$, Supporting Information Fig. S8 and Supporting Information Table S2), representing a clear DOM response to *P. antarctica* cell lysis during bloom decline. This DOC increase aligns with the $9 \pm 6\%$ DOC production previously reported for the ASP (Chen et al. 2019). Second, optical signatures show a strong DOM response through the dominance of protein-like fluorescence components ($C_{260/288}$, $C_{270/324}$, $C_{275/340}$) and mycosporine-like amino acid (MAA)-associated CDOM peaks, matching patterns observed in prior studies (Chen et al. 2019; Hu et al. 2023). Third, at the molecular level, the DOM response manifests as enrichment of labile compounds (lipids, proteins) and low-molecular-weight molecules (< 350 Da: 30.3% in ASP vs. 20.9% in CDW, Fig. 8), consistent with size exclusion chromatography results (Chen et al. 2019). While methodological differences prevent direct quantitative comparisons between studies, the skewed molecular weight distribution toward smaller metabolites (Fig. 8a) provides compelling evidence for the DOM response dominated by *P. antarctica*-derived compounds like glycolipids and peptides during bloom senescence. Additionally, DOM in the ASP exhibits significantly higher diversity, evenness, and lability indices (e.g., AI_{mod}, I_{DEG}) compared to OW and SIC, consistent with fresher, more labile DOM derived from *P. antarctica* bloom senescence (Supporting Information Table S2 and Supporting Information Fig. S9). Together, these patterns demonstrate how DOM composition and characteristics respond dynamically to phytoplankton bloom collapse in polar marine systems.

Sulfur-containing DOM molecules are significantly higher in the ASP than in open water and ice-covered areas ($p < 0.05$). Dimethylsulfoniopropionate (DMSP) released by *P. antarctica* is oxidized to dimethylsulfide (DMS), and further to dimethyl sulfoxide (DMSO). Potentially driving biogeochemical reactions that enhance sulfur-containing DOM (Hopkins et al. 2023). While methionine ($C_5H_{11}NO_2S$, MW = 149), a bacterial protein incorporating sulfur from DMSP (Kiene et al. 2000), was not detected in this study; FT-ICR-MS analysis identified its oxidized derivative, methionine sulfone ($C_5H_{11}NO_4S$). Two factors may explain this

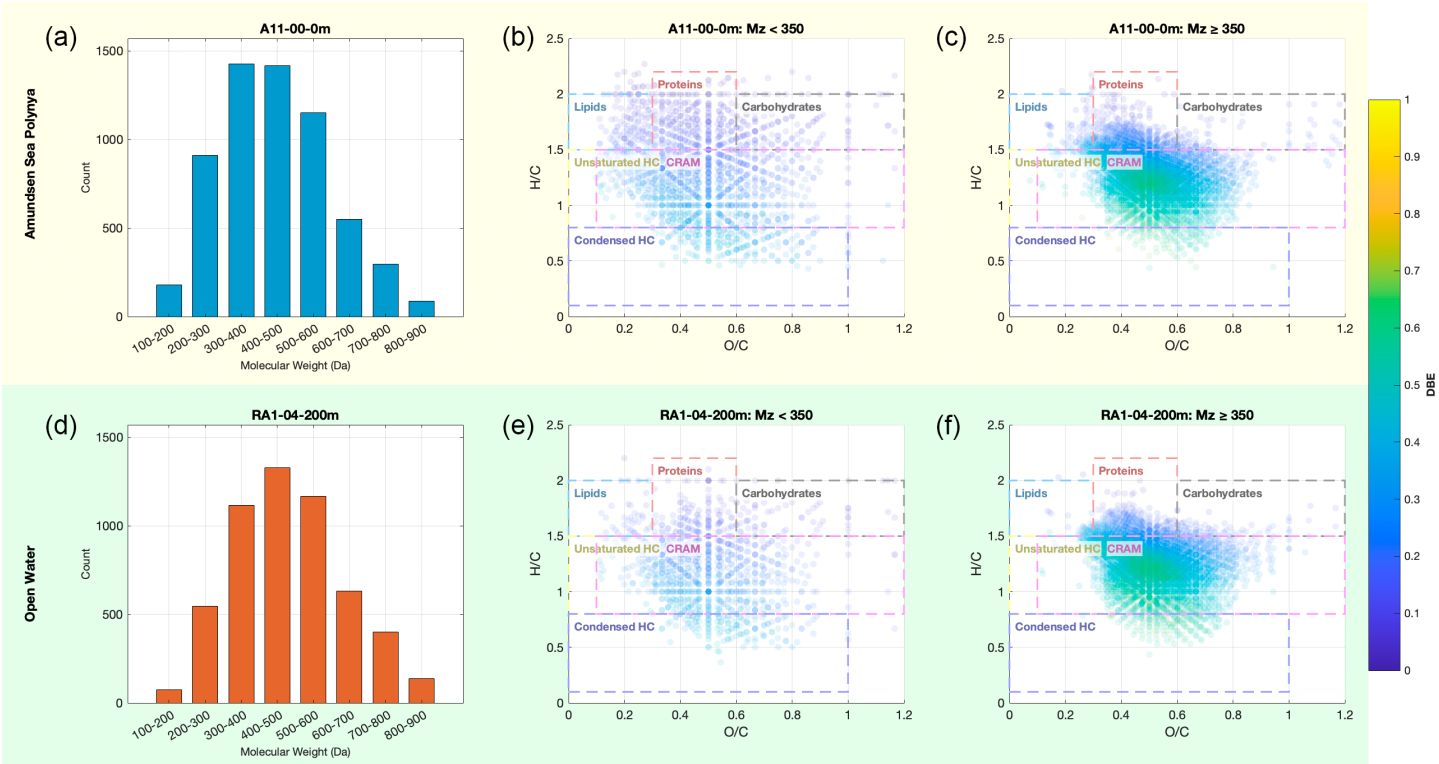

Fig. 8. Molecular weight distribution histograms (**a**, **d**) and Van Krevelen diagrams (**b**, **c**, **e**, **f**) of SPE-DOM from Amundsen Sea Polynya (A11-00-0m, upper panels) and Open Water (RA1-04-200m, bottom panels) samples, with mass-to-charge ratio (m/z) thresholds of < 350 (b, e) and ≥ 350 (c, f), illustrating the relative abundance and compositional classification of organic compounds including lipids (cyan), proteins (red), carbohydrates (black), CRAM (pink), and condensed hydrocarbons (purple).

observation: First, FT-ICR MS has reduced sensitivity for low-molecular-weight molecules like methionine (MW 149), which may fall near the instrument's detection threshold. Second, the ASP's strong oxidative conditions likely promote rapid methionine oxidation to methionine sulfone. Methionine sulfone's distribution—concentrated in the upper 100 m of the ASP and surface ice-covered areas (Supporting Information Fig. S7)—closely aligns with MLB_L pattern (Fig. 7g) and phytoplankton growth rates (Fig. 2b). Its absence at 200 m depth suggests oxidative processes are surface-driven, consistent with photochemical or microbial activity in the polynya.

While this study captures a key phase of bloom-driven DOM cycling, it is inherently limited to late summer; future seasonal or high-frequency observations, from pre-bloom through peak and collapse, are essential to resolve the full trajectory of DOM production, transformation, and fate. Moreover, integrating DOM characterization with microbial community profiling (e.g., metagenomics) is needed to elucidate DOM–microbe interactions. Such efforts will improve estimates of carbon sequestration efficiency in the ASP, a climate-sensitive hotspot where expanding polynyas may enhance productivity but not necessarily long-term carbon export due to the remineralization of labile DOM.

Author Contributions

Hui Lin: Conceptualization, Data curation, Sample collection, Sample analysis, Writing—original draft preparation, Writing—review and editing. Qiang Hao: Writing—review and editing. Wei Zhang: Sample analysis. Zhenwei Yan: Sample analysis, Data curation. Hao Zhang and Yuan Gao: Sample collection. Ziming Fang: Data curation, Writing—review and editing. Ding He: Data curation, Writing—review and editing. Yong Yu: Conceptualization, Writing—review and editing.

Acknowledgments

The authors thank the crew of R/V icebreaker *Xuelong* for their assistance in sample collection and analysis on board. The authors offer special thanks to Dr. Weidong Kong for his insighful suggestions to this manuscript. We also thank the Institute of Environmental Physics, University of Bremen for the provision of the merged MODIS-AMSR2 sea-ice concentration data at https://data.seaice.uni-bremen.de/modis_amsr2. This work was financially supported by the National Natural Science Foundation of China (42506256), Key Research & Development Program of the Ministry of Science and Technology of China (Grant No. 2022YFC2807600), the Research Grants Council of the Hong Kong Special Administrative Region, China (16306623), and the Center for Ocean Research in Hong Kong and Macau (CORE). CORE is a joint research center for ocean research between Laoshan Laboratory and HKUST.

Conflicts of Interest

None declared.

Data Availability Statement

All relevant data supporting the findings of this study are available within Supporting Information Tables S3–S6.

References

Arrigo, K. R., K. E. Lowry, and G. L. van Dijken. 2012. "Annual Changes in Sea Ice and Phytoplankton in Polynyas of the Amundsen Sea, Antarctica." *Deep Sea Research Part II: Topical Studies in Oceanography* 71, no. 76: 5–15. https://doi.org/10.1016/j.dsr2.2012.03.006.

Arrigo, K. R., G. van Dijken, and S. Pabi. 2008. "Impact of a Shrinking Arctic Ice Cover on Marine Primary Production." *Geophysical Research Letters* 35: L19603. https://doi.org/10.1029/2008GL035028.

Arrigo, K. R., and G. L. van Dijken. 2003. "Phytoplankton Dynamics Within 37 Antarctic Coastal Polynya Systems." *Journal of Geophysical Research: Oceans* 108: 3271. https://doi.org/10.1029/2002jc001739.

Bender, S. J., D. M. Moran, M. R. McIlvin, et al. 2018. "Colony Formation in *Phaeocystis antarctica*: Connecting Molecular Mechanisms With Iron Biogeochemistry." *Biogeosciences* 15: 4923–4942. https://doi.org/10.5194/bg-15-4923-2018.

Chen, M., and R. Jaffé. 2016. "Quantitative Assessment of Photo- and Bio-Reactivity of Chromophoric and Fluorescent Dissolved Organic Matter From Biomass and Soil Leachates and From Surface Waters in a Subtropical Wetland." *Biogeochemistry* 129: 273–289. https://doi.org/10.1007/s10533-016-0231-7.

Chen, M., J. Jung, Y. K. Lee, T. W. Kim, and J. Hur. 2019. "Production of Tyrosine-Like Fluorescence and Labile Chromophoric Dissolved Organic Matter (DOM)and Low Surface Accumulation of Low Molecular Weight-Dominated DOM in a Productive Antarctic Sea." *Marine Chemistry* 213: 40–48. https://doi.org/10.1016/j.marchem.2019.04.009.

D'Andrilli, J., W. T. Cooper, C. M. Foreman, and A. G. Marshall. 2015. "An Ultrahigh-Resolution Mass Spectrometry Index to Estimate Natural Organic Matter Lability." *Rapid Communications in Mass Spectrometry* 29: 2385–2401. https://doi.org/10.1002/rcm.7400.

Dittmar, T., B. Koch, N. Hertkorn, and G. Kattner. 2008. "A Simple and Efficient Method for the Solid-Phase Extraction of Dissolved Organic Matter (SPE-DOM) From Seawater." *Limnology and Oceanography: Methods* 6: 230–235. https://doi.org/10.4319/lom.2008.6.230.

D'Sa, E. J., H.-C. Kim, S.-Y. Ha, and I. Joshi. 2021. "Ross Sea Dissolved Organic Matter Optical Properties During an Austral Summer: Biophysical Influences." *Frontiers in Marine Science* 8: 1–18. https://doi.org/10.3389/fmars.2021.749096.

Fang, L., S. H. Lee, S. A. Lee, et al. 2020. "Removal of Refractory Dissolved Organic Carbon in the Amundsen Sea, Antarctica." *Scientific Reports* 10: 1–8. https://doi.org/10.1038/s41598-020-57870-6.

Flerus, R., O. J. Lechtenfeld, B. P. Koch, et al. 2012. "A Molecular Perspective on the Ageing of Marine Dissolved Organic Matter." *Biogeosciences* 9: 1935–1955. https://doi.org/10.5194/bg-9-1935-2012.

Golledge, N. R., E. D. Keller, A. Gossart, et al. 2025. "Antarctic Coastal Polynyas in the Global Climate System." *Nature Reviews Earth and Environment* 6: 126–139. https://doi.org/10.1038/s43017-024-00634-x.

Hertkorn, N., R. Benner, M. Frommberger, et al. 2006. "Characterization of a Major Refractory Component of Marine Dissolved Organic Matter." *Geochimica et Cosmochimica Acta* 70: 2990–3010. https://doi.org/10.1016/j.gca.2006.03.021.

Hopkins, F. E., S. D. Archer, T. G. Bell, P. Suntharalingam, and J. D. Todd. 2023. "The Biogeochemistry of Marine Dimethylsulfide." *Nature Reviews Earth & Environment* 4: 361–376. https://doi.org/10.1038/s43017-023-00428-7.

Hu, J., S. Xue, J. Zhao, et al. 2023. "Dynamics of Chromophoric Dissolved Organic Matter in a Highly Productive Amundsen Sea Polynya." *Marine Chemistry* 257: 104329. https://doi.org/10.1016/j.marchem.2023.104329.

Jacobs, S., A. Jenkins, H. Hellmer, et al. 2012. "The Amundsen Sea and the Antarctic Ice Sheet." *Oceanography* 25: 154–163. https://doi.org/10.5670/oceanog.2012.90.

Jeon, M. H., J. Jung, M. O. Park, S. Aoki, T. W. Kim, and S. K. Kim. 2021. "Tracing Circumpolar Deep Water and Glacial Meltwater Using Humic-like Fluorescent Dissolved Organic Matter in the Amundsen Sea, Antarctica." *Marine Chemistry* 235: 104008. https://doi.org/10.1016/j.marchem.2021.104008.

Jiang, B., J. Zhao, D. Li, et al. 2024. "Molecular Composition Evolution of Dissolved Organic Matter With Water Depth in Prydz Bay of East Antarctic: Carbon Export Implications." *Journal of Geophysical Research: Oceans* 129: 1–12. https://doi.org/10.1029/2023JC020571.

Kiene, R. P., L. J. Linn, and J. A. Bruton. 2000. "New and Important Roles for DMSP in Marine Microbial Communities." *Journal of Sea Research* 43: 209–224. https://doi.org/10.1016/S1385-1101(00)00023-X.

Koch, B. P., and T. Dittmar. 2006. "From Mass to Structure: An Aromaticity Index for High-Resolution Mass Data of Natural Organic Matter." *Rapid Communications in Mass Spectrometry* 20: 926–932. https://doi.org/10.1002/rcm.2386.

Koch, B. P., and T. Dittmar. 2016. "Erratum: From Mass to Structure: An Aromaticity Index for High-Resolution Mass Data of Natural Organic Matter." *Rapid Communications in Mass Spectrometry* 30: 250. https://doi.org/10.1002/rcm.7433.

LaRowe, D. E., and P. Van Cappellen. 2011. "Degradation of Natural Organic Matter: A Thermodynamic Analysis." *Geochimica et Cosmochimica Acta* 75: 2030–2042. https://doi.org/10.1016/j.gca.2011.01.020.

Lee, S. H., J. Hwang, H. W. Ducklow, et al. 2017. "Evidence of Minimal Carbon Sequestration in the Productive Amundsen Sea Polynya." *Geophysical Research Letters* 44: 7892–7899. https://doi.org/10.1002/2017GL074646.

Lee, Y., J. Jung, T. W. Kim, E. J. Yang, and J. Park. 2022. "Phytoplankton Growth Rates in the Amundsen Sea (Antarctica) During Summer: The Role of Light." *Environmental Research* 207: 112165. https://doi.org/10.1016/j.envres.2021.112165.

Lewis, K. M., A. E. Arntsen, P. Coupel, et al. 2019. "Photoacclimation of Arctic Ocean Phytoplankton to Shifting Light and Nutrient Limitation." *Limnology and Oceanography* 64: 284–301. https://doi.org/10.1002/lno.11039.

Li, S., J. L. Yang, G. Q. Zhao, Z. Li Ling, X. Rao, and H. L. Huang. 2025. "Spatiotemporal Characteristics of Population Structure for Antarctic Krill (Euphausia Superba) during Austral Summer in Amundsen Sea." *Advances in Polar Science* 36: 124–136. https://doi.org/10.12429/j.advps.2024.0025.

Ludwig, V., G. Spreen, and L. T. Pedersen. 2020. "Evaluation of a New Merged Sea-Ice Concentration Dataset at 1 km Resolution From Thermal Infrared and Passive Microwave Satellite Data in the Arctic." *Remote Sensing* 12: 3183. https://doi.org/10.3390/rs12193183.

Macdonald, G. J., S. F. Ackley, A. M. Mestas-Nuñez, and A. Blanco-Cabanillas. 2023. "Evolution of the Dynamics, Area, and Ice Production of the Amundsen Sea Polynya, Antarctica, 2016–2021." *The Cryosphere* 17: 457–476. https://doi.org/10.5194/tc-17-457-2023.

Mohrmann, M., C. Heuzé, and S. Swart. 2021. "Southern Ocean Polynyas in CMIP6 Models." *The Cryosphere* 15: 4281–4313. https://doi.org/10.5194/tc-15-4281-2021.

Murphy, K. R., C. A. Stedmon, D. Graeber, and R. Bro. 2013. "Fluorescence Spectroscopy and Multi-Way Techniques. PARAFAC." *Analytical Methods* 5: 6557–6566. https://doi.org/10.1039/c3ay41160e.

Ortega-Retuerta, E., T. K. Frazer, C. M. Duarte, et al. 2009. "Biogeneration of Chromophoric Dissolved Organic Matter by Bacteria and Krill in the Southern Ocean." *Limnology and Oceanography* 54: 1941–1950. https://doi.org/10.4319/lo.2009.54.6.1941.

Park, J., F. I. Kuzminov, B. Bailleul, et al. 2017. "Light Availability Rather than Fe Controls the Magnitude of Massive Phytoplankton Bloom in the Amundsen Sea Polynyas, Antarctica." *Limnology and Oceanography* 62: 2260–2276. https://doi.org/10.1002/lno.10565.

Riegger, L., and D. Robinson. 1997. "Photoinduction of UV-Absorbing Compounds in Antarctic Diatoms and *Phaeocystis antarctica*." *Marine Ecology Progress Series* 160: 13–25. https://doi.org/10.3354/meps160013.

Ross, R. M., L. B. Quetin, T. Newberger, and S. A. Oakes. 2004. "Growth and Behavior of Larval Krill (*Euphausia superba*) Under the Ice in Late Winter 2001 West of the Antarctic Peninsula." *Deep Sea Research Part II: Topical Studies in Oceanography* 51: 2169–2184. https://doi.org/10.1016/j.dsr2.2004.07.001.

Seidel, M., P. L. Yager, N. D. Ward, et al. 2015. "Molecular-Level Changes of Dissolved Organic Matter along the Amazon River-to-Ocean Continuum." *Marine Chemistry* 177: 218–231. https://doi.org/10.1016/j.marchem.2015.06.019.

Shen, Y., and R. Benner. 2019. "Molecular Properties Are a Primary Control on the Microbial Utilization of Dissolved Organic Matter in the Ocean." *Limnology and Oceanography* 65: 1061–1071. https://doi.org/10.1002/lno.11369.

Smith, W. O., and S. Trimborn. 2024. "Phaeocystis: A Global Enigma." *Annual Review of Marine Science* 16: 417–441. https://doi.org/10.1146/annurev-marine-022223-025031.

Spencer, R. G. M., L. Bolton, and A. Baker. 2007. "Freeze/Thaw and pH Effects on Freshwater Dissolved Organic Matter Fluorescence and Absorbance Properties From a Number of UK Locations." *Water Research* 41: 2941–2950. https://doi.org/10.1016/j.watres.2007.04.012.

Steinberg, D. K., N. B. Nelson, C. A. Carlson, and A. Prusak. 2004. "Production of Chromophoric Dissolved Organic Matter (CDOM) in the Open Ocean by Zooplankton and the Colonial Cyanobacterium *Trichodesmium* Spp." *Marine Ecology Progress Series* 267: 45–56. https://doi.org/10.3354/meps267045.

Turner, J., A. Orr, G. H. Gudmundsson, et al. 2017. "Atmosphere–Ocean–Ice Interactions in the Amundsen Sea Embayment, West Antarctica." *Reviews of Geophysics* 55: 235–276. https://doi.org/10.1002/2016RG000532.

Williams, W. J., E. C. Carmack, and R. G. Ingram. 2007. "Chapter 2: Physical Oceanography of Polynyas." In Elsevier Oceanography Series, 55–85. Elsevier. https://doi.org/10.1016/S0422-9894(06)74002-8.

Wormald, M. R., and R. A. Dwek. 1999. "Glycoproteins: Glycan Presentation and Protein-Fold Stability." *Structure* 7: R155–R160. https://doi.org/10.1016/S0969-2126(99)80095-1.

Yager, P. L., R. M. Sherrell, S. E. Stammerjohn, et al. 2012. "ASPIRE: The Amundsen Sea Polynya International Research Expedition." *Oceanography* 25: 40–53. https://doi.org/10.5670/oceanog.2012.73.

Yi, Y., C. He, K. Klaproth, et al. 2023. "Will Various Interpretation Strategies of the Same Ultrahigh-Resolution Mass Spectrometry Data Tell Different Biogeochemical Stories? A First Assessment Based on Natural Aquatic Dissolved Organic Matter." *Limnology and Oceanography: Methods* 21: 320–333. https://doi.org/10.1002/lom3.10548.

Supporting Information

Additional Supporting Information may be found in the online version of this article.

Submitted 13 August 2025
Revised 01 January 2026
Accepted 15 April 2026